Indexing of individual single-walled carbon nanotubes from Raman spectroscopy

T. Michel,[1] M. Paillet,[1] D. Nakabayashi,[1] M. Picher,[1] V. Jourdain,[1] J. C. Meyer,[2,*] A. A. Zahab,[1] and J.-L. Sauvajol[1]
[1]*Université Montpellier 2, Laboratoire des Colloides, Verres et Nanomatériaux (UMR CNRS 5587), 34095 Montpellier, France*
[2]*Max Planck Institute for Solid State Research, Stuttgart, Germany*
(Received 6 July 2009; revised manuscript received 15 October 2009; published 10 December 2009)

From combined Raman spectroscopy and electron diffraction studies on several freestanding single-walled carbon nanotubes (SWNTs), we define Raman criteria which correlate the main features of the Raman spectrum (radial breathing mode and G modes) and the optical transition energies with the structure of the SWNT under investigation. On this basis, we discuss the possibilities to determine the (n,m) indices of an individual SWNT from a single wavelength Raman experiment. We show the efficiency of this approach in assigning the (n,m) structure of different individual nanotubes including all types of achiral SWNTs. Finally, the limits and the accuracy of the method are discussed.

DOI: 10.1103/PhysRevB.80.245416 PACS number(s): 78.67.Ch, 78.30.Na, 73.22.−f

I. INTRODUCTION

For a long time, Raman spectroscopy has been widely used to derive information on the structural, vibrational, and electronic properties of single-walled carbon nanotubes (SWNTs). To this aim, several Raman experiments were performed on SWNT bundles, ensembles of individual SWNTs, individual and spatially isolated SWNTs. Radial breathing mode (RBM) and G modes are the two main features of the Raman spectrum of SWNTs.

The RBM frequency (ω_{RBM}) depends on the SWNT diameter (for a review see Ref. 1). Experimental results in the literature, regarding different kinds of SWNTs, fit well the RBM frequency vs diameter relation $\omega_{\mathrm{RBM}}=\mathbf{A}/\mathbf{d}+\mathbf{B}$ (d is the tube diameter). The factor **B** is usually associated to environmental effects (bundling, surfactant used for nanotubes dispersion, substrate) and then is expected to be zero for negligible environmental effects.

The features of the longitudinal optical (LO) and transverse optical (TO) G modes (line shape and frequency of each component) depend on tube diameter and chirality.[2,3] Consequently, information about the G modes can only be derived with a good accuracy from Raman experiments performed on individual and index-identified SWNTs. So, in spite of the investigations performed on a large number of supposedly individual SWNTs,[4] only recently the features of G modes of few semiconducting[5] and metallic[6] SWNTs have been measured from experiments performed on individual, spatially isolated, index-identified freestanding SWNTs. The frequencies of G modes can be compared with the most recent predictions about the diameter and chirality dependence of G-mode frequencies calculated by DFT method using adiabatic[2,3] and nonadiabatic assumptions.[3]

The measurement of the excitation profile of RBM gives information on the resonance transition energies (E^R) of SWNTs (see Refs. 7–10). Associated to the evaluation of the diameter of SWNTs (from the RBM frequency vs diameter relation), the knowledge of the experimental E^R allows to identify the (n,m) structure of the SWNTs from the comparison with the optical transition energies calculated in different tight-binding approaches.[7–10] Excitation profiles on ensemble of individual SWNTs give a precise (n,m) assignment from the geometrical pattern recognition between the experimental and a calculated resonance chart,[11,12] in agreement with photoluminescence studies.[13] By contrast, when the measurement of a single SWNT is done by using a single wavelength, wrong (n,m) assignment has been reported, as discussed in Ref. 14. This procedure then requires more accurate criteria including the main features of the Raman spectrum (RBM and G modes) for the indexation of a single individual nanotube measured with a single laser excitation energy.

A few years ago we developed an approach combining Raman spectroscopy and electron diffraction (ED) experiments on individual, spatially isolated, and freestanding SWNTs.[15] This approach allowed us to measure, in air and room temperature, the RBM and the G-modes features, as well as to evaluate with a good accuracy the transition energies of few individual semiconducting and metallic index-identified freestanding SWNTs.[5,15,16] The optical transitions of individual index-identified freestanding SWNTs have also been measured by Rayleigh scattering[17] and RBM excitation profiles.[18] It should be emphasized that the Raman[5,18] and Rayleigh[17] results are in very good agreement,[16] although related to independent measurements on individual index-identified freestanding SWNTs prepared in different ways. From these results, we can define Raman criteria enabling to identify, in most cases, the structure of a SWNT from its Raman features only, without the need of such techniques as electron diffraction, Rayleigh scattering or tunable Raman microscopy. The (n,m) assignment by using a single excitation wavelength can sometimes be unambiguous or lead to two or three possibilities for the (n,m) indices. In this paper, these criteria are used to (n,m) assign individual SWNTs, their domain of validity and the limits of the method are discussed.

II. RAMAN CRITERIA TO IDENTIFY INDIVIDUAL FREESTANDING SINGLE-WALLED CARBON NANOTUBES

Combined electron diffraction and Raman experiments have been performed on individual freestanding SWNTs as follows:[15] (i) two kinds of freestanding SWNTs are used:

nanotubes suspended between electrodes[15] or across holes of a membrane.[19] (ii) Before the Raman experiments, overview transmission electron microscopy (TEM) images are recorded in order to determine the position and orientation of nanotubes. (iii) Raman spectra are measured on those located nanotubes at fixed excitation energy in the ($\parallel$ $\parallel$) configuration [$\parallel$ means that the laser (scattered) polarization is along the tube axis]. With these experimental conditions, the measurement of a Raman signal in the RBM range by using a short acquisition time (typically 10 s) means that the excitation laser energy is in (quasi) coincidence with the transition energy of the tube under investigation.[5,16] (iv) The (n,m) identification of the tubes for which a Raman signal was measured is obtained from electron diffraction.[20] It must be noted that ED and high-resolution TEM (HRTEM) imaging permit also to know unambiguously if the Raman experiments were performed on individual nanotubes, double-walled nanotubes, or small bundles. In this section, the presented results were obtained on SWNTs identified from their diffraction patterns.[20]

A. RBM frequency vs diameter relationship

The first Raman experiments, at the single nanotube level, were performed on individual and spatially isolated SWNTs prepared on a silicon substrate by a chemical vapor deposition (CVD) method[21] following the pioneer study of Duesberg *et al.*[22] performed on small bundles. Subsequently, a lot of investigations were performed on ensemble of individual nanotubes such as: SWNTs wrapped with surfactant and dispersed in aqueous solution,[7–9] and carpetlike freestanding SWNTs prepared by alcohol-assisted[23] or water-assisted (supergrowth)[24] CVD method. In all these investigations, the identification of the (n,m) indices of the tubes was obtained by comparing the Raman resonance energies, derived from the measurements of the excitation profile of the RBM, and the transition energies calculated in the framework of different tight-binding approaches.

From the first experiments performed on individual and spatially isolated SWNTs on a silicon substrate, a famous relation $\omega_{\mathrm{RBM}}=\mathbf{248}/\mathbf{d}$ was obtained[21] and used in a large number of studies to derive the tube diameter from the measurement of ω_{RBM}. It must be pointed out that (i) this relation has been demonstrated to lead to wrong (n,m) assignments and (ii) that it is not valid for freestanding SWNTs. From investigations performed on ensemble of individual SWNTs prepared in different ways, the relation $\omega_{\mathrm{RBM}}=\mathbf{A}/d+\mathbf{B}$ was found but with many different values of A and B factors (depending on the kind of investigated nanotubes and environmental conditions).[14,25] Recently, the $\omega_{\mathrm{RBM}}=\mathbf{227}/d$ relation was derived from Raman experiments performed on a dense forest of long SWNTs, vertically aligned from a silicon substrate, grown by the water-assisted CVD method.[14]

In contrast to all these previous investigations, our method allows to measure the RBM frequencies of precisely identified (n,m) SWNTs. In this way, independently on any modelization of nanotube electronic properties, the ω_{RBM} vs diameter relationship

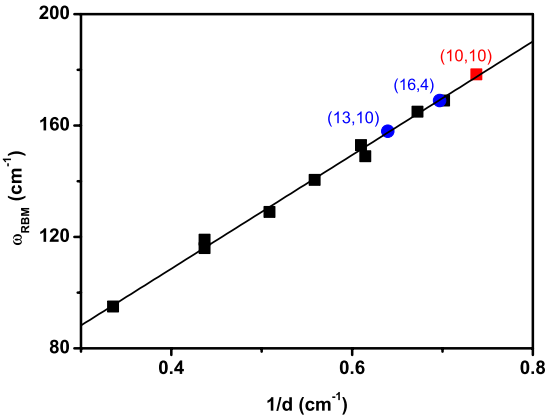

FIG. 1. (Color online) RBM frequency vs inverse diameter for nanotubes identified by electron diffraction (black squares from Ref. 15, red square for the (10,10) SWNT, blue circles from Ref. 18). Black line: $\omega_{\mathrm{RBM}}=\frac{204}{d}+27$ from Ref. 15.

$$\omega_{\mathrm{RBM}}=\frac{204}{d}+27 \tag{1}$$

was found for in air individual freestanding SWNTs in the 1.3–3 nm diameter range.[15] Equation (1) is displayed on Fig. 1 with previous experimental results (black squares). This plot includes recent data from Débarre *et al.*[18] (Fig. 1, blue dots) obtained on the index-identified freestanding (16,4) and (13,10) metallic SWNTs. Figure 1 also displays the recent measurement of a (10,10) SWNT (Fig. 1, red square) identified from ED (see also Fig. 3). For this latter SWNT, the RBM was measured at 178 cm^{-1}. The good agreement between all sets of independent data must be emphasized and shows the reliability of the ω_{RBM} vs diameter relationship when the SWNTs are suspended in air. As suggested in Refs. 14 and 26, the additional term can be understood as due to the interaction between the suspended tubes and surrounding air[27] (the discussion about the effect of air is beyond the scope of this paper). In the following, we use this relation to derive the diameters of in air freestanding SWNTs from the measurement of their RBM frequencies.

B. Line shape of the G modes

In Fig. 2, we compare the G-mode range of the Raman spectra measured on the (11,10) semiconducting SWNT (Fig. 2, top) and the (15,6) metallic SWNT (Fig. 2, bottom). These tubes have close diameters: 1.42 nm for the (11,10) and 1.46 nm for the (15,6). As expected for ($\parallel$ $\parallel$) spectrum of a chiral tube,[28–30] the G band displays two components, each of them is assigned to a A symmetry mode. In the (11,10) semiconducting tube, the profile of each component is narrow and symmetric (Fig. 2, top). The high-frequency mode at 1591 cm^{-1} is assigned to LO mode and the low frequency at 1566 cm^{-1} to TO mode. By contrast, in the (15,6) metallic tube, a broad low-frequency mode is found at 1566 cm^{-1} and a narrow high-frequency mode is located at 1591 cm^{-1}. In agreement with theoretical works,[2,3] the high-frequency mode is assigned to the TO mode and the low-frequency mode to the LO mode, the opposite of semiconducting nano-

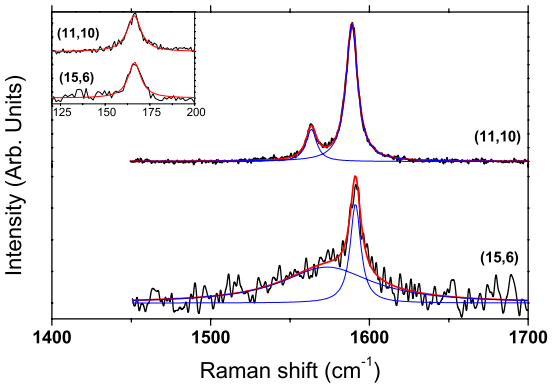

FIG. 2. (Color online) G-mode range of the Raman spectrum of two individual nanotubes with close diameters: semiconducting (11, 10) (E_{laser}=2.41 eV) and metallic (15, 6) (E_{laser}=1.7 eV). The two tubes are identified from their diffraction patterns. Inset: corresponding RBMs.

tubes. The softening (with respect to the LO mode of semiconducting SWNT) and broadening of LO component of metallic tubes are related to a Kohn anomaly at the Γ point of the Brillouin zone[3] and resonance between phonon and electron-hole pairs.[31] In terms of characterization, the line shape of the low-frequency component clearly identifies the semiconducting or metallic character of the tube under investigation. For achiral nanotubes, only one G mode of A_{1g} symmetry is Raman active.[28,29] This component is assigned to the TO mode for armchair SWNT and to the LO mode for zigzag SWNT. Figure 3 displayed the RBM (inset) and G modes ranges measured on the (10,10) SWNT. In agreement with theoretical predictions, only a single component is measured on the G-mode range of the (10,10) SWNT and assigned as the TO G mode.[3] This component is sharp, symmetric, and located at high frequency: 1598 cm^{-1}. Note that the profiles of G modes of chiral and armchair metallic SWNTs are in agreement with those measured by Wu *et al.*[6] on metallic SWNTs identified from their optical transitions measured by Rayleigh scattering. As a result, the number of component for the G band is also a criterion for the identification of a SWNT. Examples of identification of chiral and

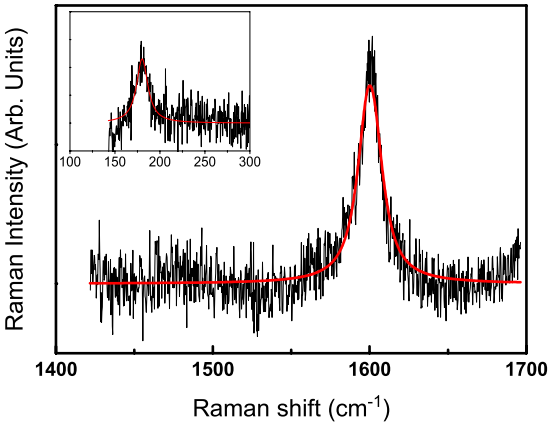

FIG. 3. (Color online) G-mode range of the Raman spectrum of the (10,10) armchair SWNT. Inset: corresponding RBM (E_{laser} =1.92 eV).

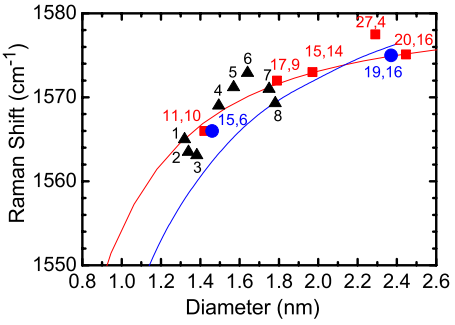

FIG. 4. (Color online) Red (blue) line: diameter dependence of the TO (LO) component of the G band for semiconducting (metallic) nanotubes calculated by Piscanec *et al.* (Ref. 3). Red (blue) dots: semiconducting (metallic) nanotubes identified from their electron-diffraction patterns. Black triangles: the diameters for tubes labeled 1–8, were obtained from their RBM frequency by using the relation (Ref. 15): $\omega_{\mathrm{RBM}}=\frac{204}{d}+27$ [the (n,m) indices of these tubes are given in Table I].

achiral SWNTs will be presented in the next section.

Concerning the diameter dependence of the TO G mode of semiconducting SWNTs, we compare in Fig. 4 our experimental data measured on semiconducting SWNTs with the recent calculations of Piscanec *et al.*[3] The good fit of the data by the Piscanec's predictions (red solid line in Fig. 4) can be used to confirm the diameter of a semiconducting tube from the measurement of its TO G-mode frequency, especially for small diameters where the diameter dependence is significant. In Fig. 4, black filled triangles represent data measured on semiconducting tubes not identified by electron diffraction. The diameters of these tubes were derived from Eq. (1). Their TO mode frequencies are in good agreement with results measured on identified SWNTs and with the calculated frequencies. In the following, the (n,m) indices of these tubes will be identified by applying our Raman criteria. Finally, as expected from calculations,[3] the frequency of the LO component of all semiconducting SWNTs investigated in this work (located around 1591 cm^{-1}) does not depend on diameter.

Until now, the G modes of index-identified metallic SWNTs have been measured on the (15,6), (19,16), and (10,10) SWNTs. The frequencies of the LO component of the (15,6) and (19,16) metallic SWNTs are found at 1566 and 1575 cm^{-1}, respectively. The agreement between the experimental (Fig. 4, blue dots) and calculated (Fig. 4, blue line) frequencies in a nonadiabatic approach[3] is reasonable. The frequencies of the TO G mode for these metallic SWNTs are systematically found around 1590 cm^{-1} as predicted in a nonadiabatic approximation. These experimental findings obtained on index identified metallic SWNTs, support the fact that both curvature and dynamic (nonadiabatic) effects should be taken into account to correctly describe the G-mode frequencies for metallic SWNTs. Indeed, when the nonadiabatic effects are not considered, the frequencies of both TO and LO modes are significantly downshifted (of about 20 cm^{-1}), in the diameter range investigated (see Figs. 16 and 19 in Ref. 3).

C. Optical transitions

The detection of a signal in the RBM range by using a short acquisition time (typically 10 s) means that the excitation laser energy is in (quasi) coincidence with the transition energy of the tube under investigation. We have been able by this way to derive the transition energies of few identified individual SWNTs, with error bars of about 30 meV corresponding to the average width of the RBM excitation profiles measured for individual freestanding SWNTs.[18] More precisely, Raman experiments[5,15] [(including those of Débarre *et al.* (Ref. 18)] and Rayleigh experiments[17] allow us to measure the first metallic transition (E_{11}^M) and the third (E_{33}^S) and fourth (E_{44}^S) semiconducting transitions for a few index-identified SWNTs in the 1.3–3 nm range. The good matching between the experimental data and the rigidly shifted transition energies (E_{ii}^N) calculated in the framework of a nonorthogonal tight-binding formalism[32] lead to the so-called normalized Kataura plot (the procedure is described in detail in Refs. 5, 16, and 26). This procedure has been extended to the second metallic transition (E_{22}^M) thanks to the Rayleigh data available.[17] This normalized Kataura plot is the key tool to identify the (n,m) structure of an individual SWNT from the knowledge of its diameter (derived from its RBM frequency) and its Raman resonance energy.

We claim that the use of these Raman criteria allow in many cases, the identification of individual SWNTs and, in most cases, the exclusion of wrong indexation. In the next section, we illustrate the efficiency of this approach to index the structure of several carbon nanotubes. We focus on three examples: (i) the (n,m) identification of chiral SWNTs, (ii) the indexation of zigzag semiconducting and metallic SWNTs, and (iii) the identification of nanotubes in bundle.

III. IDENTIFICATION OF THE STRUCTURE OF INDIVIDUAL FREESTANDING SWNTS

A. Identification of individual SWNTs

In Fig. 5 (top), we show the Raman spectrum of a nanotube in resonance with the 2.41 eV excitation energy. A single RBM is located at 174.6 cm^{-1} giving a diameter of 1.38 nm for this SWNT [according to Eq. (1)]. The G-mode line shape is the one of a chiral semiconducting nanotube with two narrow components located at 1563 cm^{-1} (TO) and 1590 cm^{-1} (LO). The frequency of the TO mode confirms the diameter of the tube (see Fig. 4). Because the RBM and G modes were detected in few seconds at the 2.41 eV excitation [step (iii) of our procedure], the optical transition of the semiconducting tube under investigation is very close of 2.41 eV. More precisely, the stronger intensity of the Stokes component with respect to the anti-Stokes component (Fig. 5, gray line, corrected by the Bose factor) suggests that this resonance energy is slightly lower than 2.41 eV. Regarding the diameter of this semiconducting tube (1.38 nm), the involved transition is the third excitonic transition. The diameter and the laser energy (2.41 eV) are reported on our normalized Kataura (red filled triangle in Fig. 5). A good matching between these features and those of the (12,8) tube (red square in Fig. 5) is found, leading to identify the tube

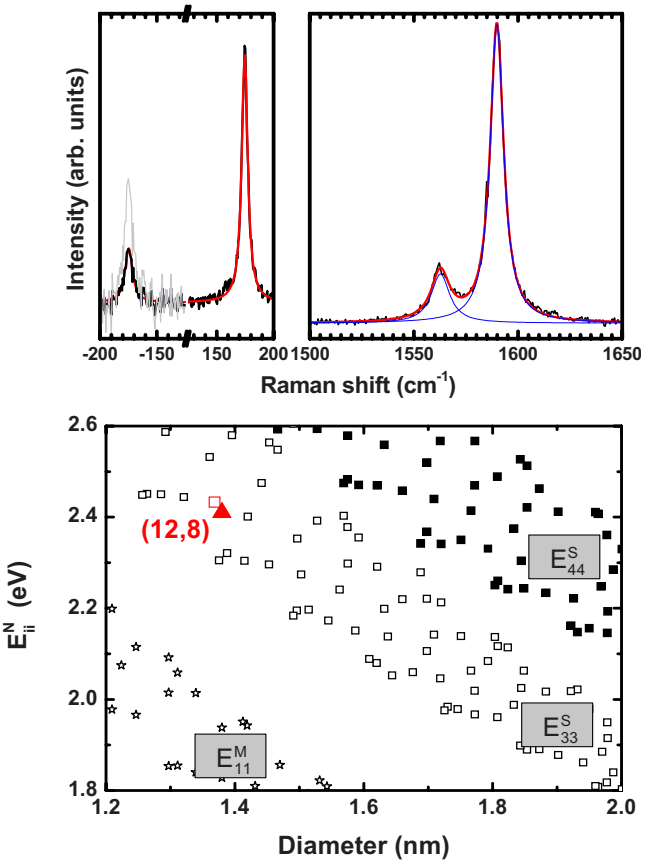

FIG. 5. (Color online) Top: RBM Stokes and anti-Stokes located at +174.6 and −174.6 cm^{-1}, respectively (left) and G mode (right) ranges of the Raman spectrum of an individual freestanding SWNT in resonance with E_{laser} at 2.41 eV. The gray line shows the anti-Stokes spectrum normalized by the Bose factor. Bottom: normalized Kataura plot (Refs. 5, 16, and 32). Black stars, open and filled squares are for calculations of the first transition of metallic tubes, the third and fourth transitions of semiconducting tubes, respectively. Red symbols are related to the energy transition of the (12,8): open large square is for calculation and filled triangle is for experiment.

under investigation as the (12,8) SWNT. A careful examination of this region of the Kataura plot rules out other assignments.

By using the same procedure, we have been able to identify all the tubes which appear in Fig. 4 (black triangles). The possible (n,m) assignment, in a reasonable diameter/energy ranges are given in the Table I. The line shape of the TO modes, associated to the presence of two components, leads to the conclusion that the tubes are chiral and semiconducting. The frequencies of the G modes are another confirmation of the diameter. The small difference in the frequencies of RBM assigned to same tubes [see, for example, tubes 1 and 2 identified as (13,6)] gives an idea about the accuracy of the measurements (estimated at ± 1 cm^{-1}) for a single freestanding SWNT as discussed in Ref. 33. For tube 5, the (19,2) and (20,0) are both acceptable if only the $(E^R, \omega_{\mathrm{RBM}})$ couple is considered. The G-mode line shape with two components eliminate the (20,0) leading to an unique index assignment as (19,2). Taking into account the uncertainty in the

TABLE I. (n,m) assignment of the nanotubes of the Fig. 4. In each case, experimental values $(d_{\mathrm{RBM}}, E_{laser})$ are compared with calculations $(E_{ii}^{N}, d_{(n,m)})$. d_{RBM} is derived from the frequency of the radial breathing mode and $d_{(n,m)}$ is calculated from the usual relation $(d=1.42\frac{\sqrt{3(n^2+m^2+nm)}}{\pi})$. Transition energies (E_{ii}^{N}) are calculated in a nonorthogonal tight-binding formalism (Ref. 32) and normalized to the Raman results (see details in Refs. 5 and 16. For tubes 6–8 (n,m) indexes in bold characters are preferred index assignments but the other possibilities cannot be totally ruled out (see text).

Label on Fig. 4	n, m indexation	ω_{RBM} (cm^{-1})	d_{RBM} (nm)	E_{laser} (eV)	E_{ii}^{N} (eV)	$d_{(n,m)}$ (nm)
Tube 1	(13,6)	181.5	1.32	2.41	2.444	1.317
Tube 2	(13,6)	179.2	1.34	2.41	2.444	1.317
Tube 3	(12,8)	174.6	1.38	2.41	2.433	1.365
Tube 4	(16,5)	164.0	1.49	2.41	2.454	1.487
Tube 5	(19,2)	156.5	1.57	2.41	2.378	1.572
Tube 6	(**16**,**8**) or (17,6)	151.0	1.64	2.41	2.458 or 2.470	1.657 or 1.618
Tube 7	(**14**,**12**) or (18,7)	143.6	1.75	2.41	2.414 or 2.350	1.765 or 1.749
Tube 8	(**17**,**9**) or (14,12)	141.5	1.78	2.41	2.331 or 2.414	1.790 or 1.765

RBM frequencies and transition energies, the possibilities for the (n,m) indexes of tube 6–8, are given in Table I. Privileged identification can be extracted (indices with bold characters) from the G-mode line shape and from the intensity of the signal. For instance, the TO/LO intensity ratio remains to be described accurately and thus definitive single index assignment cannot always be drawn.

B. Identification of individual zigzag SWNTs

We now turn to examples where only a single component is measured in the G-mode range. Figure 6 displays the Raman spectra of two suspended SWNTs in close resonance with the 2.41 eV excitation energy. The RBM of these tubes are located at 132.2 and 135.1 cm^{-1} giving diameters close to 1.94 and 1.89 nm, respectively. The line shape of G band consists in a single narrow component for one (Fig. 6 left, top) and a single, slightly asymmetric and broad component for the other one (Fig. 6 left, bottom). The presence of a single G mode unambiguously states that the both tubes investigated are achiral. Reporting the diameter and the excitation energy of each tube on the normalized Kataura plot (see Fig. 6, right), we observe that only two achiral zigzag tubes are present in this diameter-energy range. With regards to the specific line shape of G modes, we assign the first one to the semiconducting zigzag (25,0) SWNT (E_{44}^{S} predicted at 2.411 eV) and the second one to the metallic zigzag (24,0) SWNT (E_{22}^{M-} predicted at 2.493 eV).

Combined with the line shape of G mode measured on the armchair (10,10) SWNT (Fig. 3), the line shapes of G mode of (24,0) and (25,0) SWNTs display the intrinsic Raman responses of the three types of achiral SWNTs.

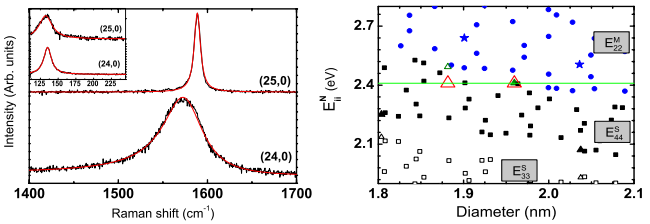

FIG. 6. (Color online) Left: G-mode range of the Raman spectrum of a (25,0) zigzag semiconducting SWNT (top) and a (24,0) zigzag metallic SWNT (bottom). The indexes are derived according to the criteria presented in this work. Inset: corresponding RBMs. Right: corresponding region of the normalized Kataura plot (Refs. 5, 16, and 32). Blue stars, blue triangles, and blue dots: E_{22}^{M} for armchair, zigzag, and chiral metallic SWNTs, respectively. Black squares and black filled squares: E_{33}^{S} and E_{44}^{S} for semiconducting chiral SWNTs, respectively. Black triangles and black filled triangles: E_{33}^{S} and E_{44}^{S} for semiconducting zigzag SWNTs. Green triangle and green filled triangle: theoretical points for the (24,0) and the (25,0), respectively. Red triangles: (d,E^{R}) parameters from Raman measurements. The horizontal green line at 2.41 eV corresponds to E_{laser}.

C. Identification of SWNTs in bundle

Figure 7(a) shows the TEM image of a long nanostructure suspended across different gaps between electrodes. We have measured the Raman spectra of this long nanostructure in the regions I and II, indicated by arrows on Fig. 7(a). The RBM and G-mode ranges of the Raman spectra measured in these two areas are displayed in Fig. 7 in panels (b) and (c), respectively.

In region I, ED experiment unambiguously identified this individual tube as a (19,16) metallic SWNT (diameter $\approx$2.37 nm). G modes were measured in the Raman spectrum excited at 2.41 eV [Fig. 7(b)]. The metallic line shape of G modes is well fitted by two Lorentzians: a broad component located at 1575 cm^{-1} (LO mode) and a narrow line at 1591 cm^{-1} (TO mode). Using the diameter dependence of the LO mode of Ref. 3, the predicted value of the diameter is around 2.4 nm in agreement with ED. In region I, no RBM was measured. For this excitation energy, the resonance condition is then achieved only for the outgoing light scattered by the G modes. As shown on the normalized Kataura plot of Fig. 7(b), we confirm the 2.41 eV laser excitation is close of

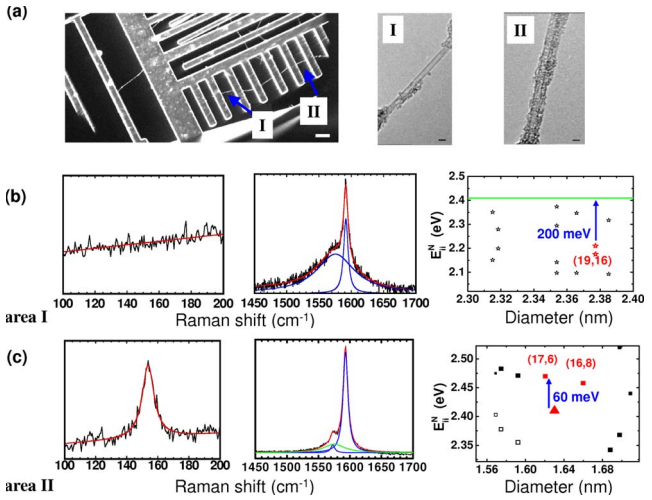

FIG. 7. (Color online) Panel (a): (left) TEM image of a long nanostructure suspended between electrodes. The blue arrows indicate the two regions (I and II) were Raman spectra have been recorded (scale bar is 1 μm). (right) HRTEM images of regions I and II (the amorphous carbon which appears in the images is deposited during TEM analysis). Scale bars are 5 nm. Panel (b): the RBM and G-mode ranges of the Raman spectrum measured in the area I of the nanotube (19,16) as identified by ED and corresponding Kataura plot (red and black stars are for calculations). The green horizontal line corresponds to E_{laser}. The blue arrow corresponds to $\hbar\omega_{Gmode}$. Panel (c): Raman spectrum obtained in the area II. Kataura plot: black and red squares are for calculations and red triangle for experiments. The blue arrow corresponds to the difference between E_{laser} (2.41 eV) and $E_{44}^{S}[(17,6)]$.

the resonance with the outgoing light scattered by the G modes

$$E_{laser} - \hbar\omega_{Gmode} = E_{22}^{M}[(19,16)],$$

where $\hbar\omega_{Gmode}$ is the G-mode phonon energy.

As shown in Fig. 7(c), a different Raman spectrum has been measured in the region II at 2.41 eV. A strong single RBM at 153 cm^{-1} is measured. Assuming this tube as individual, its diameter is found close to 1.62 nm using Eq. (1). On the other hand, the G-mode profile is close to the one measured on semiconducting tubes, with two dominant narrow lines located at 1572.5 and 1593 cm^{-1} [Fig. 7(c)]. However, the presence of a weak broad band, located at the same position than the LO mode of the (19,16) tube [solid green line in the Fig. 7(c)] suggests the presence of a bundle in the region II. The TO component of the (19,16) tube is very likely merged with the LO component of the semiconducting tube. In summary, we evidenced by Raman spectroscopy that the (19,16) metallic tube is bundled with a semiconducting tube in region II.

Reporting the couple (d, E^R) of this tube, namely (1.62 nm, 2.41 eV), on the normalized Kataura plot, we find that the transition energy is redshifted of about 60 meV with regard to the transitions energy calculated for the individual tubes located in the same region of the Kataura plot, namely (17,6) and (16,8), SWNTs [Fig. 7(c), left]. This redshift confirms that the experiment in region II was performed on a bundle. Indeed, Raman[18,34,35] and Rayleigh[36] experiments carried out on individual tubes and bundles showed that the interaction between the tubes in small bundle (2–3 tubes)[18,35,36] redshifts the transition energies of SWNTs compared to their individual form by a value of about 50 meV.[37]

In summary, we showed that the analysis of the profile of the G modes and the transition energy can evidence the bundling. (n,m) assignment of the tubes forming the bundle will be done and discussed in the next section.

D. Discussion

We discuss in this section the possible sources of error in the (n,m) assignment of tubes using our approach and the consequences if the Raman criteria are not fulfilled. On one hand, the methodology presented here is limited by the accuracy of Eq. (1) and of the normalized Kataura plot. One can find some cases where SWNTs are not spaced enough to give an unambiguous indexation between two tubes (see, for instance, Table I). However, the G-modes profile allows to discriminate the chiral or achiral character as illustrated in the previous section, thus reducing the number of possibilities for the (n,m) indices. The method presented here should then not be taken as universal to determine the (n,m) indexes in all cases but the consistency between RBM, G mode, and E^R should allow to rule out wrong indexation in a single wavelength Raman experiment in a large majority of the cases.

On the other hand, sources of error can be separated between extrinsic factors such as environment, doping, experimental conditions, and intrinsic factor related to the nanostructure itself (e.g., like bundling). These points are discussed in the following.

In the previous section, from the analysis of the G modes and the transition energy, we have shown the presence of a bundle in region II of Fig. 7(a). The two possible semiconducting tubes that form the bundle have slightly different diameters: 1.618 nm [RBM predicted at 153.1 cm^{-1} from Eq. (1)] and 1.657 nm (RBM predicted at 150.1 cm^{-1}) for the (17,6) and the (16,8), respectively. Consequently, as we measure a RBM at 153 cm^{-1} we propose to identify the bundled semiconducting tube as the (17,6) SWNT. However, if Eq. (1) (established for individual tubes) leads to an under estimation of the diameter of tubes forming the bundle, we cannot rule out definitively the (16,8) tube. Moreover, from the Raman data only, the possibility that other nonresonant (at 2.41 eV) SWNTs is part of this bundle cannot be discarded. The Raman experiment has been completed by TEM imaging performed on the two regions of Fig. 7(a). A single (19,16) SWNT is observed in region I and is suspended in the other regions. In region II, TEM imaging confirms that this tube is bundled with another one. The measurement by ED of the equatorial line of the bundled part shows the coexistence of two diameters: 2.35 ± 0.05 nm associated to the (19,16) metallic tube and 1.64 ± 0.05 nm in complete agreement with the preceding conclusion. This example shows that indexation from Raman spectroscopy could sometimes be possible but we believe that TEM analysis is necessary to ensure that another nonresonant nanotube is not present in

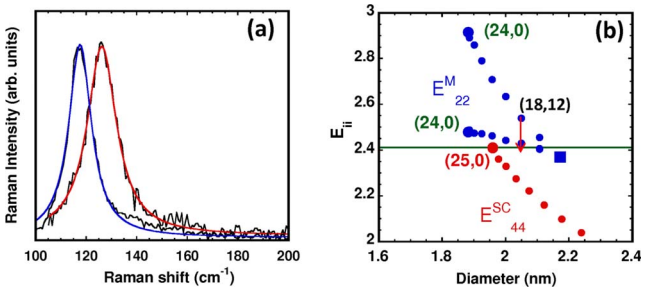

FIG. 8. (Color online) (a) RBM range of the Raman spectra measured on the same suspended nanotube using two different powers densities 15 kW cm^{-2} (red line) and 60 kW cm^{-2} (blue line). E_{laser}=2.41 eV. (b) Corresponding region of the normalized Kataura plot. Vertical arrow indicates the redshift of the transition energy under laser-induced heating.

the bundle or to distinguish between a bundle of SWNTs and small multi-walled carbon nanotubes .[35,37]

Environmental effects play a major role in the disparity of the results about G modes of metallic SWNTs found in the literature.[3] As shown previously, the profile of the LO G mode of individual metallic SWNT is broad and asymmetric. It is usually described by a Breit-Wigner-Fano (BWF) profile.[6] However, the shift of the Fermi level related to the doping of individual metallic SWNTs leads to a significant narrowing of the LO G mode because of the decreasing of the resonance between the phonon and the electronic excitations.[38,39] For instance, the narrowing and upshift of the BWF component of the LO mode reported in Ref. 40 measured on a tube lying on a silicon substrate is due to an accidental doping of the SWNTs under investigation. Then, a knowledge and the control of the environmental conditions is important in the (n,m) assignment of SWNTs.

Another possible source of errors is related to experimental conditions. Figure 8 (left) displays the RBMs measured for an individual SWNT suspended over a hole on a silicon membrane at the 2.41 eV excitation energy. Two measurements were performed for two different values of the power density impinging on the nanotube. The spectrum taken with a power of about 15 kW/cm^2 (blue line) shows a RBM located at 126 cm^{-1}. The diameter derived from the usual relation is close to 2.05 nm. Reporting this diameter and the 2.41 eV energy in the corresponding region of the Kataura plot (Fig. 8, right) shows that this nanotube can be assigned as the (18,12). The G-mode range of the Raman spectrum confirms this assignment (not shown). For a measurement performed at 60 kW/cm^2 on the same nanotube the RBM frequency is downshifted to 117.6 cm^{-1}. This downshift is attributed to the heating of the tube by the laser. More striking is the narrowing of the RBM under heating: the FWHM is 12 cm^{-1} for the lowest power density and 8.5 cm^{-1} for the highest power density. We can explain this result by a redshift of the transition energy under laser-induced heating as previously reported in the literature.[41] The heating induced by the laser causes the transition energy to be lowered of a few meV leading to a better achievement of the resonance condition and consequently, a narrowing of the RBM linewidth.[42] This example shows that measurements at the single nanotube level require a perfect control of the experimental conditions.

Finally, to determine unambiguously the (n,m) indices of a SWNT, all the criteria discussed above must all be fulfilled together. If one of the criteria is not consistent with the other ones it means that the tube investigated is in bundle, doped, or simply that it is not a SWNT.

IV. CONCLUSION

Based on combined Raman and experiments data, we have stated several Raman criteria which allow the Raman identification of semiconducting and metallic freestanding SWNTs at room temperature and in air from a single wavelength Raman experiment. In order to illustrate the efficiency of this approach we have reported the (n,m) identification of individual chiral and achiral freestanding SWNTs and the identification of tubes organized in a small individual bundle. This study emphasizes the ability and the difficulties of the resonant Raman spectroscopy as a metrological method for the characterization of carbon nanotubes. Concerning the G mode of metallic SWNTs, our measurements support the description of the Raman spectrum of these nanotubes in a nonadiabatic theory. Further improvements of the method could be obtained by studying, for example, the 2D mode behavior as a function of (n,m).

ACKNOWLEDGMENTS

The authors thank S. Piscanec, R. Arenal, G. Moussaed, L. Henrard, and V. N. Popov for support and helpful discussions. This work has been done in the framework of the GDR-E No. 2756 "Science and Application of the Nanotubes-NANO-E." The authors acknowledge financial support by the ANR projects "Nanotubes suspendus" and T-NICE.

*Present address: Electron microscopy of materials science, University of Ulm, Albert-Einstein-Allee 11, 89143 Ulm, Germany.

[1] S. Reich, C. Thomsen, and J. Maultzsch, *Carbon Nanotubes: Basic Concepts and Physical Properties* (Wiley-VCH, Weinheim, Germany, 2004).

[2] O. Dubay, G. Kresse, and H. Kuzmany, Phys. Rev. Lett. **88**, 235506 (2002).

[3] S. Piscanec, M. Lazzeri, J. Robertson, A. C. Ferrari, and F. Mauri, Phys. Rev. B **75**, 035427 (2007).

[4] A. Jorio, A. G. Souza Filho, G. Dresselhaus, M. S. Dresselhaus, A. K. Swan, M. S. Unlu, B. Goldberg, M. A. Pimenta, J. H. Hafner, C. M. Lieber, and R. Saito, Phys. Rev. B **65**, 155412 (2002).

[5] M. Paillet, T. Michel, J. C. Meyer, V. N. Popov, L. Henrard, S. Roth, and J.-L. Sauvajol, Phys. Rev. Lett. **96**, 257401 (2006).

[6] Y. Wu, J. Maultzsch, E. Knoesel, B. Chandra, M. Huang, M. Y.

Sfeir, L. E. Brus, J. Hone, and T. F. Heinz, Phys. Rev. Lett. **99**, 027402 (2007).
[7] C. Fantini, A. Jorio, M. Souza, M. S. Strano, M. S. Dresselhaus, and M. A. Pimenta, Phys. Rev. Lett. **93**, 147406 (2004).
[8] H. Telg, J. Maultzsch, S. Reich, F. Hennrich, and C. Thomsen, Phys. Rev. Lett. **93**, 177401 (2004).
[9] M. S. Strano, S. K. Doorn, E. H. Haroz, C. Kittrell, R. H. Hauge, and R. E. Smalley, Nano Lett. **3**, 1091 (2003).
[10] P. T. Araujo, S. K. Doorn, S. Kilina, S. Tretiak, E. Einarsson, S. Maruyama, H. Chacham, M. A. Pimenta, and A. Jorio, Phys. Rev. Lett. **98**, 067401 (2007).
[11] J. Maultzsch, H. Telg, S. Reich, and C. Thomsen, Phys. Rev. B **72**, 205438 (2005).
[12] S. K. Doorn, D. A. Heller, P. W. Barone, M. L. Usrey, and M. S. Strano, Appl. Phys. A: Mater. Sci. Process. **78**, 1147 (2004).
[13] S. M. Bachilo, M. S. Strano, C. Kittrell, R. H. Hauge, R. E. Smalley, and R. B. Weisman, Science **298**, 2361 (2002).
[14] P. T. Araujo, I. O. Maciel, P. B. C. Pesce, M. A. Pimenta, S. K. Doorn, H. Qian, A. Hartschuh, M. Steiner, L. Grigorian, K. Hata, and A. Jorio, Phys. Rev. B **77**, 241403(R) (2008).
[15] J. C. Meyer, M. Paillet, T. Michel, A. Moreac, A. Neumann, G. S. Duesberg, S. Roth, and J.-L. Sauvajol, Phys. Rev. Lett. **95**, 217401 (2005).
[16] T. Michel, M. Paillet, J. C. Meyer, V. N. Popov, L. Henrard, and J.-L. Sauvajol, Phys. Rev. B **75**, 155432 (2007).
[17] M. Y. Sfeir, F. Wang, L. Huang, C.-C. Chuang, J. Hone, S. P. O'Brien, T. F. Heinz, and L. E. Brus, Science **306**, 1540 (2004).
[18] A. Débarre, M. Kobylko, A. M. Bonnot, A. Richard, V. N. Popov, L. Henrard, and M. Kociak, Phys. Rev. Lett. **101**, 197403 (2008).
[19] V. Jourdain (unpublished).
[20] J. C. Meyer, M. Paillet, G. S. Duesberg, and S. Roth, Ultramicroscopy **106**, 176 (2006).
[21] A. Jorio, R. Saito, J. H. Hafner, C. M. Lieber, M. Hunter, T. McClure, G. Dresselhaus, and M. S. Dresselhaus, Phys. Rev. Lett. **86**, 1118 (2001).
[22] G. S. Duesberg, I. Loa, M. Burghard, K. Syassen, and S. Roth, Phys. Rev. Lett. **85**, 5436 (2000).
[23] Y. Murakami, E. Einarsson, T. Edamura, and S. Maruyama, Carbon **43**, 2664 (2005).
[24] K. Hata, D. N. Futaba, K. Mizuno, T. Namai, M. Yumura, and S. Iijima, Science **306**, 1362 (2004).
[25] A. Jorio, M. S. Dresselhaus, and G. Dresselhaus, *Carbon Nanotubes: Advanced Topics in Synthesis, Properties, and Application*, Topics in Applied Physics Vol. 11 (Springer, Berlin, 2008).
[26] T. Michel, M. Paillet, J. C. Meyer, V. Popov, L. Henrard, P. Poncharal, A. Zahab, and J.-L. Sauvajol, Phys. Status Solidi B **244**, 3986 (2007).
[27] M. J. Longhurst and N. Quirke, J. Chem. Phys. **124**, 234708 (2006).
[28] R. Saito, T. Takeya, T. Kimura, G. Dresselhaus, and M. S. Dresselhaus, Phys. Rev. B **57**, 4145 (1998).
[29] A. Rahmani, J.-L. Sauvajol, S. Rols, and C. Benoit, Phys. Rev. B **66**, 125404 (2002).
[30] J. Jiang, R. Saito, K. Sato, J. S. Park, Ge. G. Samsonidze, A. Jorio, G. Dresselhaus, and M. S. Dresselhaus, Phys. Rev. B **75**, 035405 (2007).
[31] M. Lazzeri, S. Piscanec, F. Mauri, A. C. Ferrari, and J. Robertson, Phys. Rev. B **73**, 155426 (2006).
[32] V. N. Popov, New J. Phys. **6**, 17 (2004); V. N. Popov and L. Henrard, Phys. Rev. B **70**, 115407 (2004).
[33] A. G. Walsh, W. Bacsa, A. N. Vamivakas, and A. K. Swan, Nano Lett. **8**, 4330 (2008).
[34] M. J. O'Connell, S. Sivaram, and S. K. Doorn, Phys. Rev. B **69**, 235415 (2004).
[35] M. Fouquet, H. Telg, J. Maultzsch, Y. Wu, B. Chandra, J. Hone, T. F. Heinz, and C. Thomsen, Phys. Rev. Lett. **102**, 075501 (2009).
[36] F. Wang, M. Y. Sfeir, L. Huang, X. M. Henry Huang, Y. Wu, J. Kim, J. Hone, S. O'Brien, L. E. Brus, and T. F. Heinz, Phys. Rev. Lett. **96**, 167401 (2006).
[37] In Ref. 35, our criteria would have been more favorable to an identification of the two tubes as a part of a DWNT with a (15,0)@semiconducting tube. This shows the difficulty to distinguish between a bundle of two SWNTs and a DWNT without TEM imaging. This could be an explanation for the much more important redshift (160 meV) deduced in Ref. 35 compared to Refs. 18 and 36.
[38] K. T. Nguyen, A. Gaur, and M. Shim, Phys. Rev. Lett. **98**, 145504 (2007).
[39] H. Farhat, H. Son, Ge. G. Samsonidze, S. Reich, M. S. Dresselhaus, and J. Kong, Phys. Rev. Lett. **99**, 145506 (2007).
[40] M. Paillet, P. Poncharal, A. Zahab, J.-L. Sauvajol, J. C. Meyer, and S. Roth, Phys. Rev. Lett. **94**, 237401 (2005).
[41] S. B. Cronin, Y. Yin, A. Walsh, R. B. Capaz, A. Stolyarov, P. Tangney, M. L. Cohen, S. G. Louie, A. K. Swan, M. S. Unlu, B. B. Goldberg, and M. Tinkham, Phys. Rev. Lett. **96**, 127403 (2006).
[42] A. Jorio, C. Fantini, M. S. S. Dantas, M. A. Pimenta, A. G. Souza Filho, Ge. G. Samsonidze, V. W. Brar, G. Dresselhaus, M. S. Dresselhaus, A. K. Swan, M. S. Unlu, B. B. Goldberg, and R. Saito, Phys. Rev. B **66**, 115411 (2002).